J Solid State Electrochem (2012) 16:2823–2836
DOI 10.1007/s10008-012-1712-9

ORIGINAL PAPER

Influence of preparation method on structure, morphology, and electrochemical performance of spherical $Li[Ni_{0.5}Mn_{0.3}Co_{0.2}]O_2$

Shunyi Yang · Xianyou Wang · Xiukang Yang · Ziling Liu · Yansong Bai · Yingping Wang · Hongbo Shu

Received: 2 November 2011 / Revised: 24 February 2012 / Accepted: 2 March 2012 / Published online: 16 March 2012

Abstract Spherical $Li[Ni_{0.5}Mn_{0.3}Co_{0.2}]O_2$ was prepared by both the continuous hydroxide co-precipitation method and continuous carbonate co-precipitation method under different calcined temperatures. The physical properties and electrochemical behaviors of $Li[Ni_{0.5}Mn_{0.3}Co_{0.2}]O_2$ prepared by two methods were characterized by X-ray diffraction, scanning electron microscope, and electrochemical measurements. It has been found that different preparation methods will result in the differences in the morphology (shape, particle size, and tap density), structure stability, and the electrochemical characteristics (shape of initial charge/discharge curve, cycle stability, and rate capability) of the final product $Li[Ni_{0.5}Mn_{0.3}Co_{0.2}]O_2$. The physical and electrochemical properties of the spherical $Li[Ni_{0.5}Mn_{0.3}Co_{0.2}]O_2$ prepared by continuous hydroxide co-precipitation is apparently superior to the one prepared by continuous carbonate co-precipitation method. The optimal sample prepared by continuous hydroxide co-precipitation at 820 °C exhibits a hexagonally ordered layer structure, high special discharge capacity, good capacity retention, and excellent rate capability. It delivers high initial discharge capacity of 175.2 mAh g^{-1} at 0.2 C rate between 3.0 and 4.3 V, and the capacity retention of 98.8 % can be maintained after 50 cycles. While the voltage range is broadened up to 2.5 and 4.6 V vs. Li^+/Li, the special discharge capacities at 0.2 C, 0.5 C, 1 C, 2 C, 5 C, and 10 C rates are as high as 214.3, 205.0, 198.3, 183.3, 160.1 and 135.2 mAh g^{-1}, respectively.

S. Yang · X. Wang (✉) · X. Yang · Z. Liu · Y. Bai · Y. Wang · H. Shu
Key Laboratory of Environmentally Friendly Chemistry and Applications of Ministry of Education, School of Chemistry, Xiangtan University,
Hunan, Xiangtan 411105, China
e-mail: wxianyou@yahoo.com

Keywords Lithium ion batteries · $Li[Ni_{0.5}Mn_{0.3}Co_{0.2}]O_2$ · Preparation method · Electrochemical behavior · Spherical morphology

Introduction

In recent years, much attention has been paid to a layered $Li[Ni_{0.5}Mn_{0.5}]O_2$ that can be considered as a one-to-one mixture of $LiNiO_2$ and $LiMnO_2$ [1–3]. It has many advantages over $LiNiO_2$ and $LiMnO_2$, such as high capacity, structural and thermal stability, and excellent cyclic performance. Nevertheless, it also has two main drawbacks. One is its difficulty in preparation by conventional solid-state method, in which Li_2MnO_3 was preferentially formed, and unreacted NiO remained [4, 5]. Another is its lower electronic conductivity, which dramatically reduces its specific capacity even at a moderate current density [6].

Cobalt doping can not only promote the formation of $Li[Ni_{0.5}Mn_{0.5-x}Co_x]O_2$ but also enhance the electronic conductivity and the thermal stability of $Li[Ni_{0.5}Mn_{0.5-x}Co_x]O_2$ [7–10]. $Li[Ni_{0.5}Mn_{0.3}Co_{0.2}]O_2$, which can be considered as one of the most promising cathode materials for the application of lithium ion battery among $Li[Ni_{0.5}Mn_{0.5-x}Co_x]O_2$ series, was first proposed by Liu et al. [11]. It was initially prepared by traditional mixed hydroxide method at 750 °C in flowing oxygen and showed the initial discharge capacity of 140 mAh g^{-1} at a current density of 0.2 mA cm^{-2} between 2.75 and 4.2 V vs. Li^+/Li. Li et al. [7, 8] prepared it by solid-state reaction at 950 °C in O_2 later and found that Co non-equivalent substitution could not only reduce the impurity phase (NiO) content, improve the crystallinity of the compound but also significantly decreased the charge transfer resistance, thereby improving the rate capabilities. However, a closer performance inspection for the samples

prepared by different technical routes reveals some contradictory information on the electrochemical behaviors such as the shape of initial charge curve, reversible capacity, and cyclic performance. This strongly implied that the electrochemical characteristics of $Li[Ni_{0.5}Mn_{0.3}Co_{0.2}]O_2$ are prone to be affected by preparation condition. In order to further improve its electrochemical performance, it is necessary to study the influence of preparation method on the structural and electrochemical characteristics of $Li[Ni_{0.5}Mn_{0.3}Co_{0.2}]O_2$ and clarify the essential reason of the difference.

In our previous work [12, 13], continuous carbonate co-precipitation method has been proven to be a good choice of for the preparation of $[Ni_{1/3}Co_{1/3}Mn_{1/3}]CO_3$ as the precursor of $LiNi_{1/3}Co_{1/3}Mn_{1/3}O_2$ cathode material with excellent performance. In this paper, both the continuous carbonate co-precipitation (CCC method) and continuous hydroxide co-precipitation (CHC method) have been adopted to prepare the spherical $Li[Ni_{0.5}Mn_{0.3}Co_{0.2}]O_2$. The effects of preparation method on the structural, morphological, and electrochemical characteristics of $Li[Ni_{0.5}Mn_{0.3}Co_{0.2}]O_2$ are comparatively studied.

Experimental

Technical route of the CHC method

The details of the co-precipitation apparatus are shown in Fig. 1. $[Ni_{0.5}Mn_{0.3}Co_{0.2}](OH)_2$ precursor was synthesized by continuous hydroxide co-precipitation process in the CSTR under N_2 atmosphere protection. Initially, the CSTR-1 was filled with distilled water corresponding to 20 vol.% of the reactor, and the pH was then adjusted to 11.0 with proper amount of NH_4OH and 3.6 M NaOH to get an initial solution. The solution was stirred at 800 rpm; the temperature of the solution was maintained at 50 °C. A 1.8-M aqueous solution of $NiSO_4{\cdot}6H_2O$, $MnSO_4{\cdot}H_2O$, and $CoSO_4{\cdot}7H_2O$ corresponding to a molar composition of Ni/Mn/Co=5:3:2 was introduced continuously into the CSTR-1. Simultaneously, a 3.6-M aqueous solution of NaOH and 0.2 M NH_4OH was separately fed into the reactor. The total feed flow rate was adjusted to assure an average residence time of 10 h in CSTR-1. The liquid product that overflowed out from the CSTR-1 was fed into CSTR-2 for ageing step, which was kept the same reaction conditions as CSTR-1. Then, the products that collected continuously from the base of CSTR-2 was filtered, washed, and dried at 110 °C for 12 h to obtain $[Ni_{0.5}Mn_{0.3}Co_{0.2}](OH)_2$ precursor. Finally, the $[Ni_{0.5}Mn_{0.3}Co_{0.2}](OH)_2$ was mixed thoroughly with 6 % excess of a stoichiometric amount of Li_2CO_3 to compensate the calcining loss. The mixture was preheated at 500 °C for 5 h and calcined at 780–900 °C for 12 h in air to obtain the final products $Li[Ni_{0.5}Mn_{0.3}Co_{0.2}]O_2$.

Technical route of the CCC method

Spherical $[Ni_{0.5}Mn_{0.3}Co_{0.2}]CO_3$ precursor was synthesized by carbonate co-precipitation process using the above device without inert atmosphere protection. The CSTR-1 was

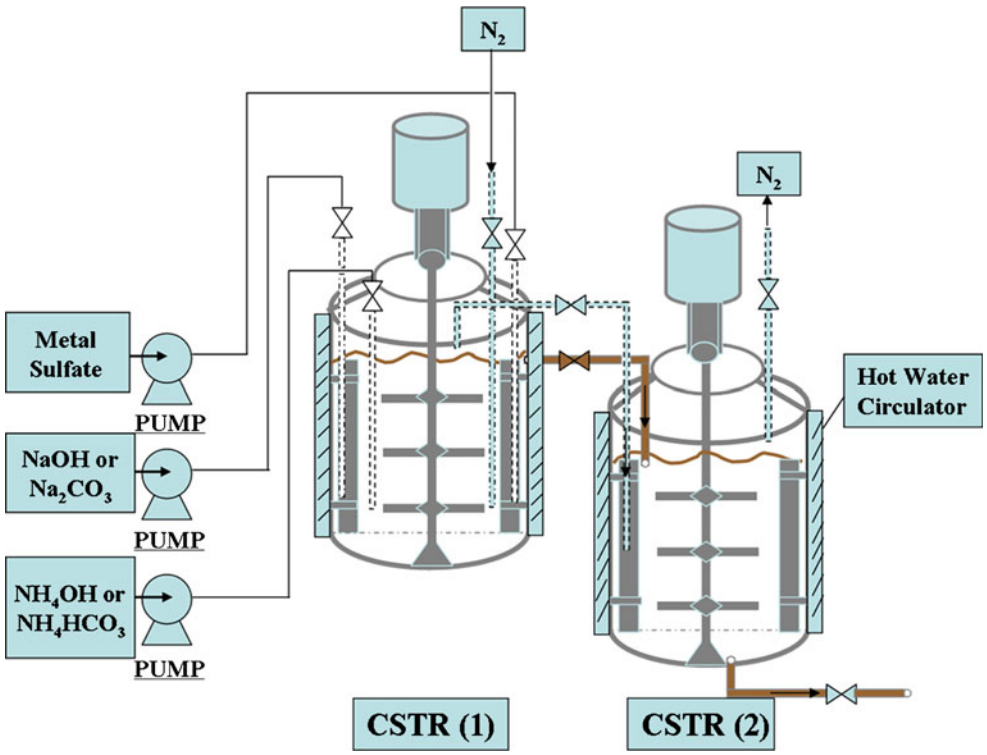

Fig. 1 Schematic of device for preparing the $[Ni_{0.5}Mn_{0.3}Co_{0.2}](OH)_2$ and $[Ni_{0.5}Mn_{0.3}Co_{0.2}]CO_3$ precursors by continuous co-precipitation

filled with distilled water corresponding to 20 vol.% of the reactor, and the pH of the water was then adjusted to 8.0 with adequate amount of NH_4HCO_3 and 1.8 M Na_2CO_3 solution. The solution was stirred at 1,000 rpm while maintaining the reactor temperature at 60 °C. A 1.8-M mixture solution of $NiSO_4{\cdot}6H_2O$, $MnSO_4{\cdot}H_2O$, and $CoSO_4{\cdot}7H_2O$ (Ni/Mn/Co=5:3:2 molar ratio) was pumped continuously into the CSTR-1. Meanwhile, a 1.8 M aqueous solution of Na_2CO_3 and 0.3 M NH_4HCO_3 was separately fed into the reactor. The total feed flow rate was adjusted to assure an average residence time of 10 h in CSTR-1. The liquid product that overflowed out from the CSTR-1 was feed into CSTR-2 for ageing step. Then, the precipitation was filtered, washed, and dried at 110 °C for 12 h to obtain $[Ni_{0.5}Mn_{0.3}Co_{0.2}]CO_3$ precursor. The $[Ni_{0.5}Mn_{0.3}Co_{0.2}]CO_3$ was fired at 500 °C for 5 h to decompose the carbonate into an oxide compound $[Ni_{0.5}Mn_{0.3}Co_{0.2}]_3O_4$. Finally, the obtained $[Ni_{0.5}Mn_{0.3}Co_{0.2}]_3O_4$ was mixed thoroughly with 6 % excess amounts of Li_2CO_3. The mixture was preheated at 500 °C for 5 h and calcined at 780–900 °C for 12 h in air to obtain $Li[Ni_{0.5}Mn_{0.3}Co_{0.2}]O_2$.

Characterization of physical and electrochemical properties

The chemical composition of the resulting powder was analyzed by atomic absorption spectroscopy (Vario 6 Analytik Jena AG, Jena, Germany). The tap density of sample was determined by Powder Integrative Characteristic Tester (BT-1000, Bettersize Instruments Ltd, China). The phase identification of the sample was performed with a diffractometer (D/Max-3 C, Rigaku, Japan). The morphology of the sample was observed using scanning electron microscopy (JSM-5600LV, JEOL, Japan). The electrochemical tests of Li $[Ni_{0.5}Mn_{0.3}Co_{0.2}O_2]$ were carried out using coin cells assembled in an argon-filled glove box. In all cells, the cathode was consisted of a mixture of active material (80 wt.%), acetylene black (10 wt.%), graphite (5 wt.%), and polyvinylidene fluoride (5 wt.%) as binder agent; lithium was served as counter and reference electrodes; a Celgard 2400 was used as separator, and the electrolyte was a 1 M $LiPF_6$ solution in ethylene carbonate (EC)-dimethyl carbonate (1:1, *V*/*V*). Charge/discharge measurements were carried out in Neware battery test system (BTS-XWJ-6.44S-00052, Newell, Shenzhen, China).

Results and discussion

Figure 2 shows the X-ray diffraction (XRD) patterns of the precursors prepared by different technical route. It can be observed that the XRD pattern of the $[Ni_{0.5}Mn_{0.3}Co_{0.2}](OH)_2$ is almost consistent with the typical fingerprint of $M(OH)_2$ (M = Ni, Mn, Co) structure [14]. All diffraction lines are indexed to a hexagonal structure with a space group of $P\bar{3}m1$. The absence of impurity phases indicates that Ni, Mn, and Co would be homogeneously distributed within $[Ni_{0.5}Mn_{0.3}Co_{0.2}](OH)_2$ particle. The co-precipitated $[Ni_{0.5}Mn_{0.3}Co_{0.2}]CO_3$ has a typical hexagonal structure with a space group of R-3c corresponding to $NiCO_3$ (JCPDS No.12-0771), of which have divalent transition metals in the formal charge [15]. The carbonate $[Ni_{0.5}Mn_{0.3}Co_{0.2}]CO_3$ was fired at 500 °C for 5 h to form $[Ni_{0.5}Mn_{0.3}Co_{0.2}]_3O_4$. The hexagonal carbonate structure has been changed to a cubic spinel Co_3O_4 structure during this process. According to the XRD patterns, the lattice parameters of *a*, *c*, and *V* were calculated by Bragg equation, and the D_{hkl} (the mean crystallite size along the (hkl) direction) was analyzed by Scherrer equation; the results were listed in Table 1. It can be found that the apparent mean crystallite size of $[Ni_{0.5}Mn_{0.3}Co_{0.2}](OH)_2$ prepared from hydroxide co-precipitation is 18.7 nm, which is two times larger than that of the precursor $[Ni_{0.5}Mn_{0.3}Co_{0.2}]_3O_4$ synthesized from carbonate co-precipitation. It is well known that the low resolution of the patterns obtained for low crystallinity/low size samples makes the application of Scherrer formula less appropriated, and so a proper refinement was needed [16, 17]. We will discuss this issue in a later paper.

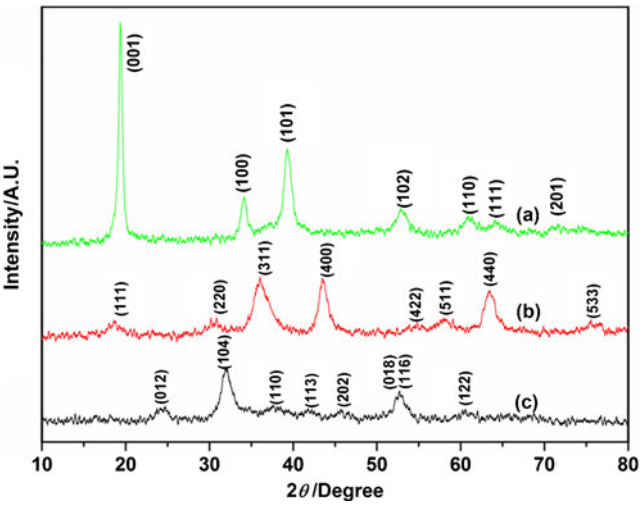

Fig. 2 XRD patterns of the precursor **a** $[Ni_{0.5}Mn_{0.3}Co_{0.2}](OH)_2$, **b** $[Ni_{0.5}Mn_{0.3}Co_{0.2}]CO_3$, and **c** $[Ni_{0.5}Mn_{0.3}Co_{0.2}]_3O_4$

Figure 3 shows the scanning electron microscope (SEM) images of the precursors synthesized by different co-precipitation processes. As being seen from Fig. 3a, c, and b, d, both the $[Ni_{0.5}Mn_{0.3}Co_{0.2}](OH)_2$ and $[Ni_{0.5}Mn_{0.3}Co_{0.2}]_3O_4$ precursors have uniform spherical morphology with an average size of about 10–15 μm. Each of the spherical particles is made up of numerous small primary grains. However, there is great deal of difference in the shape of the primary particles due to different technical route. It can be clearly seen from Fig. 3e that the primary particle of $[Ni_{0.5}Mn_{0.3}Co_{0.2}](OH)_2$ is a laminated flake minicrystal, but

Table 1 Comparison of compositions, calculated structure parameters, and tap densities for precursors synthesized by different methods

Sample	Composition	*a*-axis (Å)	*c*-axis (Å)	Unit volume (Å^3)	Crystallite size (nm)	Tap density (g cm^{-3})
$[Ni_{0.5}Mn_{0.3}Co_{0.2}]CO_3$	$[Ni_{0.501}Mn_{0.296}Co_{0.203}]CO_3$	4.763	15.235	299.310	9.1 (D_{104})	1.80
$[Ni_{0.5}Mn_{0.3}Co_{0.2}]_3O_4$	$[Ni_{0.501}Mn_{0.296}Co_{0.203}]_3O_4$	8.319	–	575.631	9.5 (D_{400})	1.87
$[Ni_{0.5}Mn_{0.3}Co_{0.2}](OH)_2$	$[Ni_{0.501}Mn_{0.297}Co_{0.202}](OH)_2$	3.056	4.582	37.058	18.7 (D_{001})	2.12

the corresponding particle in $[Ni_{0.5}Mn_{0.3}Co_{0.2}]_3O_4$ is an acicular minicrystal as shown in Fig. 3f. In addition, the tap density of the $[Ni_{0.5}Mn_{0.3}Co_{0.2}](OH)_2$ synthesized by hydroxide co-precipitation process reaches 2.12 g cm^{-3}, of which the value is higher than the $[Ni_{0.5}Mn_{0.3}Co_{0.2}]_3O_4$ precursor prepared from carbonate co-precipitation process (as shown in Table 1).

The chemical compositions of the precursors were analyzed by atomic absorption spectroscopy; the results were listed in Table 1. The AAS analysis identifies that the element ratios of Ni/Mn/Co for $[Ni_{0.5}Mn_{0.3}Co_{0.2}](OH)_2$, $[Ni_{0.5}Mn_{0.3}Co_{0.2}]CO_3$, and $[Ni_{0.5}Mn_{0.3}Co_{0.2}]_3O_4$ are 0.501:0.297:0.202, 0.501:0.296:0.203, and 0.501:0.296:0.203, respectively; the element ratio of Ni/Mn/Co is very close to 5:3:2, which is almost the same as the designed value.

Figure 4a illustrates the XRD patterns of the samples calcined at different temperatures through CHC method. Hereafter, the obtained products were labeled as CHC-780, CHC-820, CHC-860, and CHC-900, respectively. Figure 4b

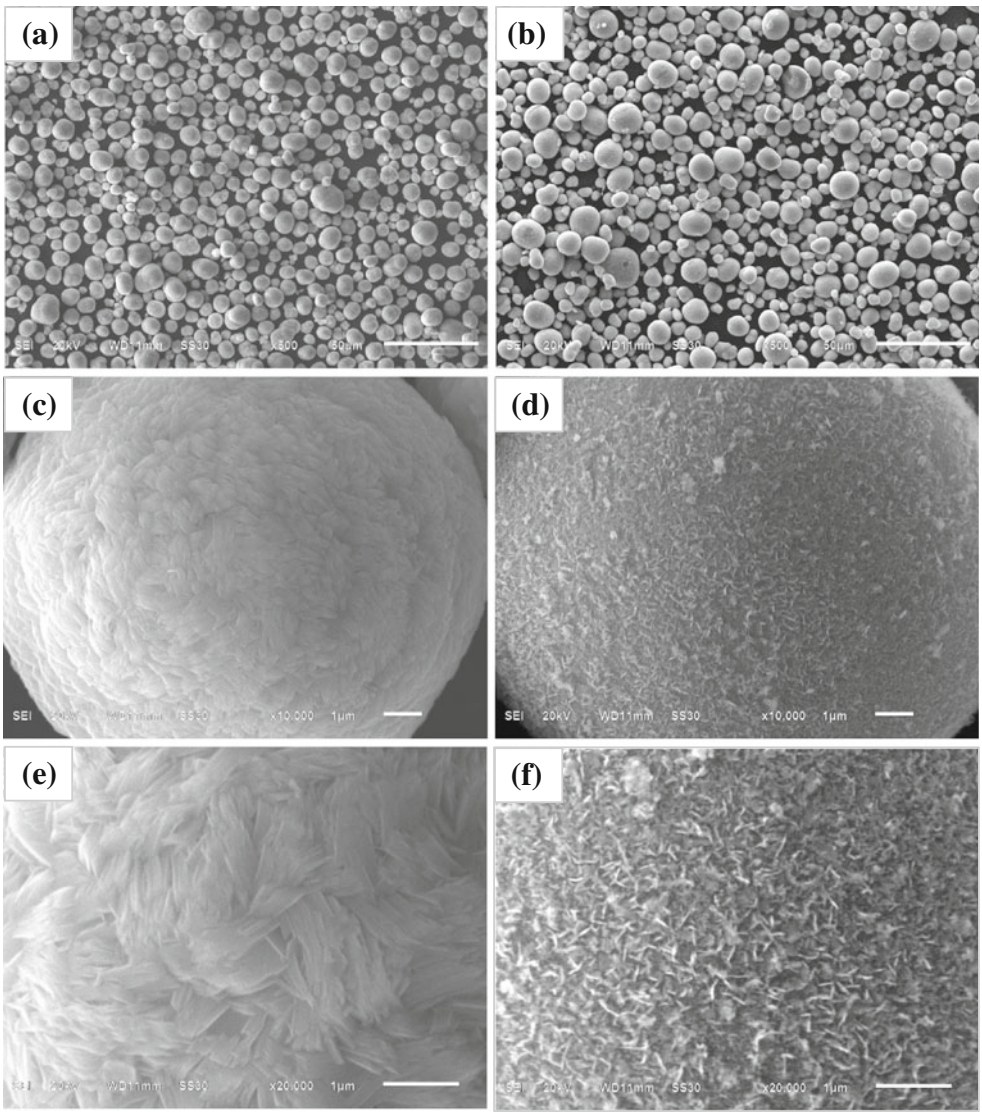

Fig. 3 SEM of the precursor **a**, **c**, **e** $[Ni_{0.5}Mn_{0.3}Co_{0.2}](OH)_2$ and **b**, **d**, **f** $[Ni_{0.5}Mn_{0.3}Co_{0.2}]_3O_4$ at different magnifications

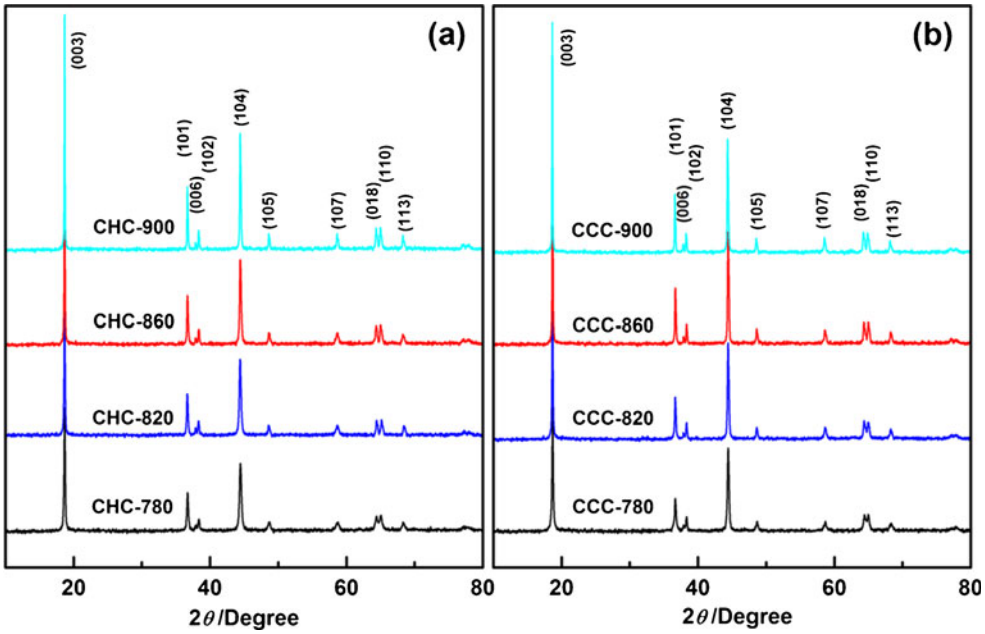

Fig. 4 XRD patterns of the Li $[Ni_{0.5}Mn_{0.3}Co_{0.2}]O_2$ powders prepared by **a** CHC method and **b** CCC method under different calcining temperatures

displays the XRD patterns of the samples prepared by CCC method calcined at different temperatures; the obtained samples were denoted as CCC-780, CCC-820, CCC-860, and CCC-900, respectively. As seen from Fig. 4, all the samples can be indexed to the hexagonal α-$NaFeO_2$ structure (space group: $R\bar{3}m$), and no impurity phase was observed in the X-ray pattern, such as NiO, which usually appear in $LiNi_{0.5}Mn_{0.5}O_2$ due to the preferential formation of Li_2MnO_3 to $LiNiO_2$ [7, 8]. In the XRD pattern, integrated peak splits of (006)/(102) and (018)/(110) are known to an indicator of characteristic of layered structure like $Li[Ni_{0.5}Mn_{0.5}]O_2$ and $Li[Ni_{1/3}Co_{1/3}Mn_{1/3}]O_2$ [2–6]. As shown in Fig. 4, for the samples prepared by CHC method, the peak splits of (006)/(102) and (018)/(110) are obviously observed above 820 °C, whereas in the samples prepared via CCC method, the clear splits of above two shoulder peaks appear up to 860 °C,

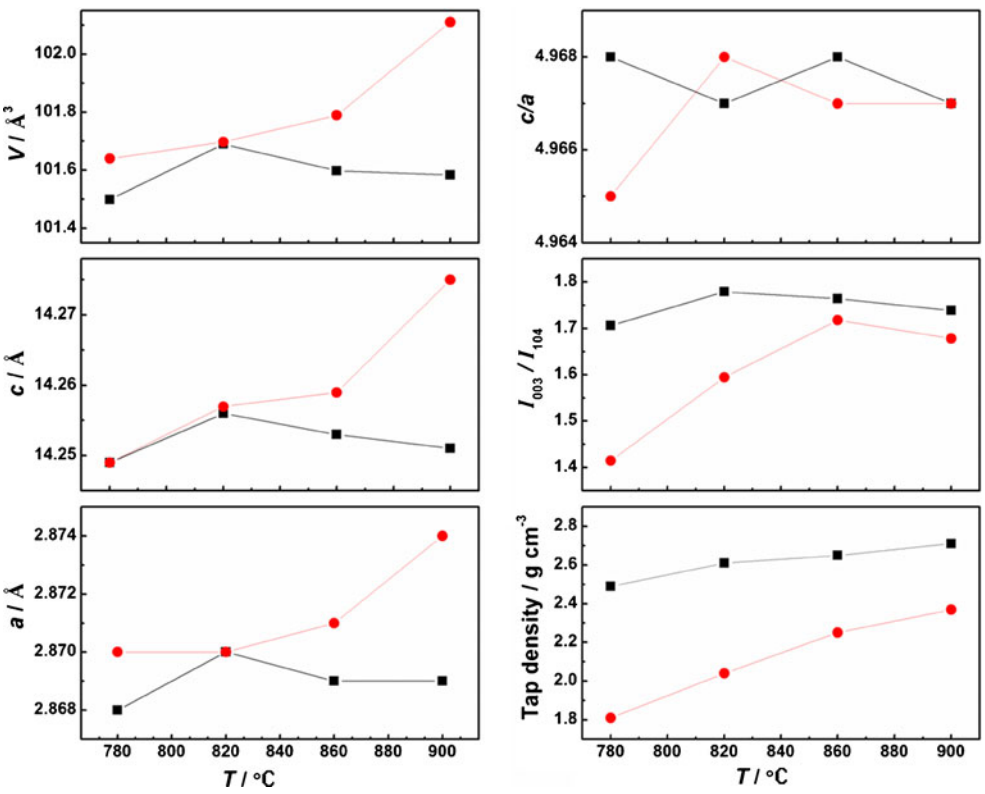

Fig. 5 Comparison of calculated structure parameters and tap densities for Li $[Ni_{0.5}Mn_{0.3}Co_{0.2}]O_2$ samples prepared by (*black squares*) CHC method and (*red circles*) CCC method under different calcining temperatures

indicating that $Li[Ni_{0.5}Mn_{0.3}Co_{0.2}]O_2$ with good layered structure can be obtained at the lower calcined temperature by CHC method than by CCC method due to the good physical properties of $[Ni_{0.5}Mn_{0.3}Co_{0.2}](OH)_2$ precursor.

According to the XRD patterns, the structure parameters of a, c, V, c/a, and I_{003}/I_{104} were calculated, and the results were illustrated in Fig. 5. As shown in Fig. 5, the lattice parameters a, c, and V of samples synthesized by CHC method have no apparent change while the calcined temperature increases. Comparatively, the lattice parameters a, c, and V of samples synthesized by the CCC method gradually increases with the increase of calcined temperature. This phenomenon indicates that the calcined temperature has great effect on the unit cell dimension of samples synthesized by

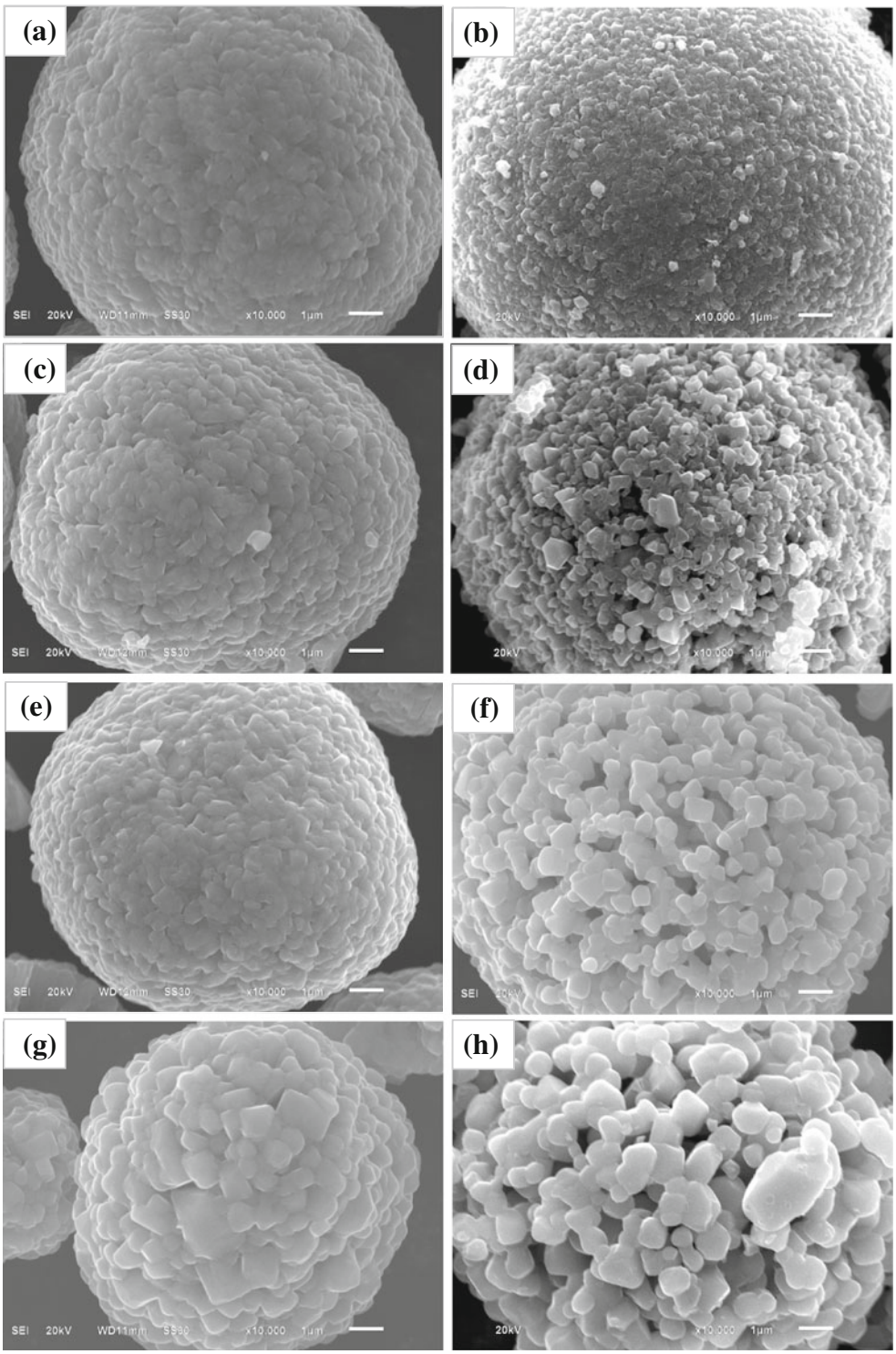

Fig. 6 SEM images of the Li $[Ni_{0.5}Mn_{0.3}Co_{0.2}]O_2$ powders prepared by CHC method and CCC method. **a** CHC-780, **c** CHC-820, **e** CHC-860, **g** CHC-900 and **b** CCC-780, **d** CCC-820, **f** CCC-860, **h** CCC-900

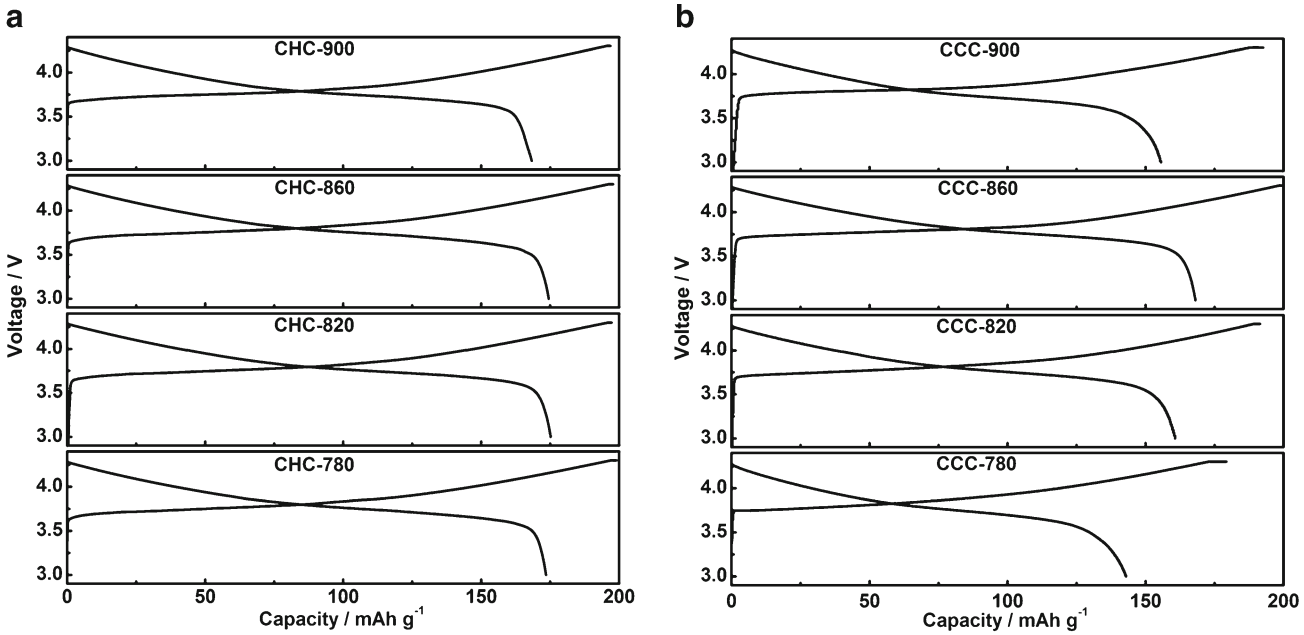

Fig. 7 The initial charge/discharge profiles of $Li[Ni_{0.5}Mn_{0.3}Co_{0.2}]O_2$ materials synthesized by **a** CHC method and **b** CCC method at 0.2 C rate in the voltage range of 3.0 and 4.3 V at 25 °C

CCC method, but little on those prepared by CHC method. It has been known that the cation mixing will deteriorate the electrochemical performance of the layered oxide materials. The integrated intensity ratio of I_{003}/I_{104} is sensitive to the cation mixing and usually taken as an approximate measure of the amount of ion mixing in the α-$NaFeO_2$ type structure materials [7–11]. It was reported that the undesirable cation mixing would appear when the ratio of I_{003}/I_{104} is smaller than 1.2 [18]. As shown in Fig. 5, the I_{003}/I_{104} values of all the samples in this work are larger than 1.2, indicating less undesirable Li^+/Ni^{2+} cation mixing exists in the as-prepared samples due to the cobalt (Co^{3+}) doping which reduce the content of Ni^{2+} in the layered $Li[Ni_{0.5}Mn_{0.3}Co_{0.2}]O_2$. This result is consistent with the previous research reported by Li et al. [7, 8]. In addition, the I_{003}/I_{104} values of the samples synthesized by the CHC method are less sensitive to the calcination temperature compared with those prepared by the CCC method. The above results reveal that the CHC method is a better alternative for the synthesis of $Li[Ni_{0.5}Mn_{0.3}Co_{0.2}]O_2$ cathode material with an ideal hexagonal layered structure.

As is well known, the surface morphology is an important influence factor for electrochemical performance of the lithium secondary batteries. Figure 6 exhibits scanning electron micrographs of $Li[Ni_{0.5}Mn_{0.3}Co_{0.2}]O_2$ samples obtained

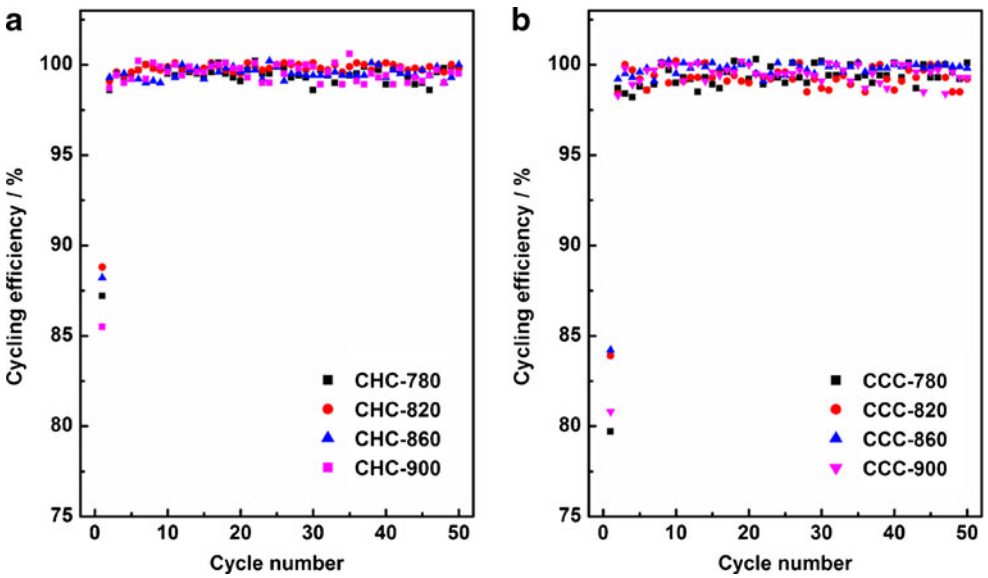

Fig. 8 Cycling efficiency as a function of cycle number for the $Li[Ni_{0.5}Mn_{0.3}Co_{0.2}]O_2$ materials synthesized by **a** CHC method and **b** CCC method at 0.2 C rate in the voltage range of 3.0 and 4.3 V at 25 °C

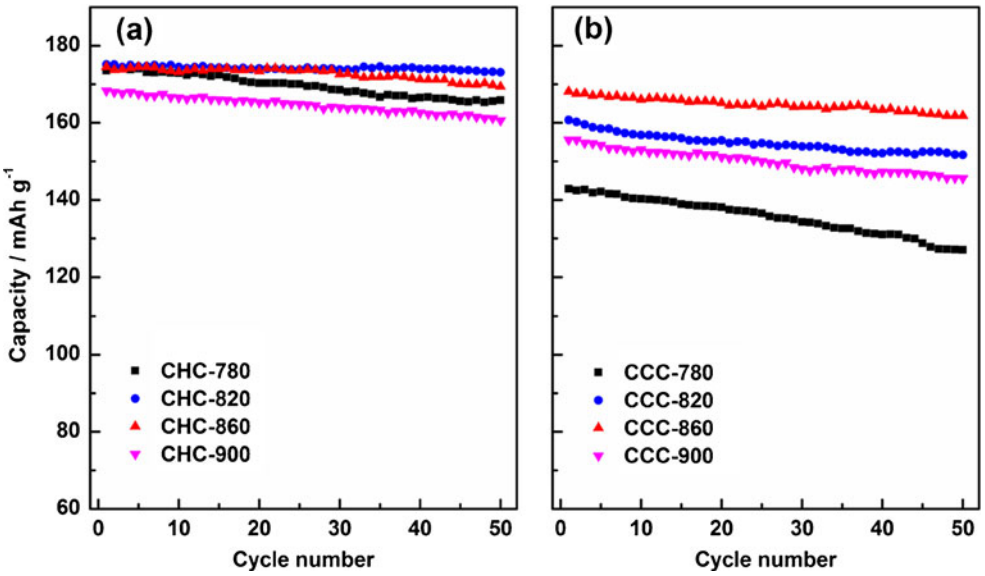

Fig. 9 Gravimetric discharge capacities as a function of cycle number for the Li $[Ni_{0.5}Mn_{0.3}Co_{0.2}]O_2$ materials synthesized by **a** CHC method and **b** CCC method at 0.2 C rate in the voltage range of 3.0 and 4.3 V at 25 °C

from different synthesis methods. As shown in Fig. 6, the secondary particles of all $Li[Ni_{0.5}Mn_{0.3}Co_{0.2}]O_2$ samples keep the spherical morphology of the precursor after the high temperature calcinations; each of the spherical particles is made up of a large number of primary grains. However, great changes have taken place on the shape of primary particle. It can be seen that the laminated flake primary particle structure of the $[Ni_{0.5}Mn_{0.3}Co_{0.2}](OH)_2$ precursor has been changed to tiny-thin plate shape (0.1–1 μm), yet the acicular primary particle of $[Ni_{0.5}Mn_{0.3}Co_{0.2}]_3O_4$ precursor is thoroughly changed to granular shape (0.1–1 μm), and the granular shapes of the primary particles slightly protrude toward the outside of the secondary structure of particles along with the temperature increasing. In comparison with the samples prepared by CCC method, the primary grains of samples prepared by CHC method stack more closely; close contact between the primary grains will benefit to get the cathode material with high tap density. It can be seen from the Fig. 5 that the tap densities of the sample CHC-780, CHC-820, CHC-860, and CHC-900 prepared by hydroxide co-precipitation reach 2.49, 2.61, 2.65, and 2.71 g cm^{-3}, respectively, of which the values are higher than the samples prepared by CCC method and the most previous results of $Li[Ni_{1/3}Co_{1/3}Mn_{1/3}]O_2$ materials [15, 19–21] and close to that of commercialized $LiCoO_2$.

In order to further study the influence of the synthesis method on the electrochemical performance of $Li[Ni_{0.5}Mn_{0.3}Co_{0.2}]O_2$, the cells were operated at 0.2 C rate (32 mA g^{-1}) for 50 cycles in the voltage range of 3.0–4.3 V vs. Li^+/Li at 25 °C. Figure 7 shows the initial charge/discharge profiles of $Li[Ni_{0.5}Mn_{0.3}Co_{0.2}]O_2$ samples synthesized by CHC and CCC methods at 0.2 C rate. As seen

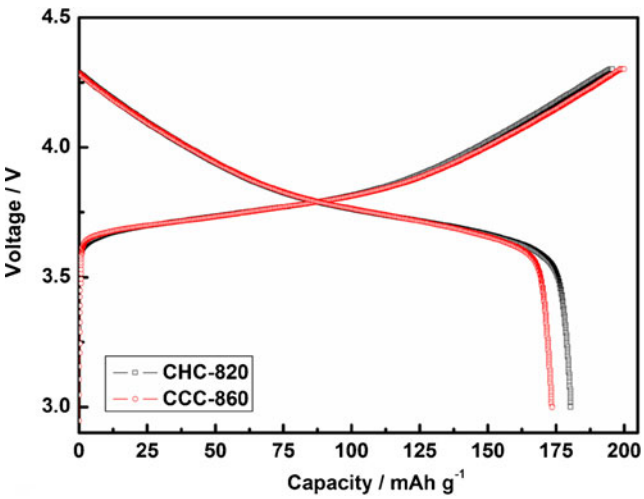

Fig. 10 The initial charge/discharge profiles for sample **a** CHC-820 and **b** CCC-860 at 0.2 C rate in the voltage range of 3.0 and 4.3 V at 55 °C

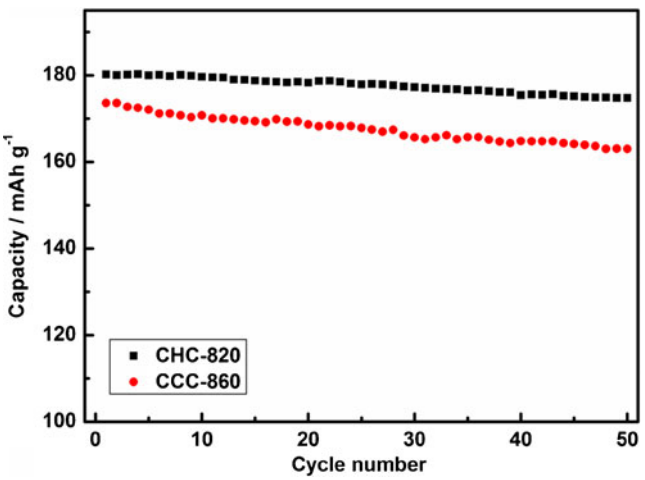

Fig. 11 Gravimetric discharge capacities as a function of cycle number for sample **a** CHC-820 and **b** CCC-860 at 0.2 C rate in the voltage range of 3.0 and 4.3 V at 55 °C

from the Fig. 7, the samples prepared by CHC method exhibit a little smaller IR drop and polarization between charge and discharge in the whole voltage range, and the operation voltage is more abruptly decayed at the end of discharge, compared with those samples prepared by CCC method. It also can be seen that the initial discharge capacity of samples prepared by CHC method depends on the heating temperature but is lower than that observed for samples prepared by CCC method. The discharge capacity increases with heating temperature up to 820 °C for the sample synthesized by CHC method and 860 °C for the sample prepared by CCC method, and then they slightly decrease above these temperatures. The initial charge and discharge capacities for the sample CHC-780, CHC-820, CHC-860, and CHC-900 are 199.0/173.5, 197.3/175.2, 197.8/174.5, and 196.8/168.3 mAh g^{-1} with a ratio of irreversible capacity loss of 12.8 %, 11.2 %, 11.8 %, and 14.5 %, respectively. By comparison, the charge and discharge capacities of 179.3/142.9, 191.5/160.7, 199.6/168.1, and 192.6/155.6 mAh g^{-1} are obtained at the first cycle for the sample CCC-780, CCC-820, CCC-860, and CCC-900, respectively, and their irreversible capacity loss reaches 20.3 %, 16.1 %, 15.8 %, and 19.2 %.

Cycling efficiencies and discharge capacities of Li$[Ni_{0.5}Mn_{0.3}Co_{0.2}]O_2$ samples as function of cycle number are presented in Figs. 8 and 9, respectively. It can be seen from Fig. 8 that all the samples show the high cycling efficiency close to 100 % upon charge and discharge cycling after the first cycle. Average efficiencies per cycle (excluding the first-cycle) of sample CHC-780, CHC-820, CHC-860, and CHC-900 synthesized by CHC method reach 99.47 %, 99.82 %, 99.63 %, and 99.49 %, respectively, while the sample CCC-780, CCC-820, CCC-860, and CCC-900 prepared by CCC method are kept at 99.19 %, 99.38 %, 99.61 %, and 99.40 %, respectively. Comparatively, the cycling efficiency of sample prepared by CHC method is higher than the sample synthesized by CCC method under the same calcining temperature, and it can hold relative steady upon cycling. As being shown in Fig. 9, the samples prepared by CHC method show the excellent cycle performance; 95.6 %, 98.8 %, 97.1 %, and 95.8 % of initial discharge capacities can be obtained after 50 cycles for sample CHC-780, CHC-820, CHC-860 and CHC-900, respectively. Compared with the samples prepared by CHC method, Li$[Ni_{0.5}Mn_{0.3}Co_{0.2}]O_2$ synthesized by CCC method exhibits the slightly inferior capacity retention under the same calcining temperature; the capacity retention after 50 cycles are 88.8 %, 94.4 %, 96.3 %, and 93.6 % for the sample CCC-780, CCC-820, CCC-860, and CCC-900, respectively. Therefore, it can be found that an optimal temperature for the synthesis of Li$[Ni_{0.5}Mn_{0.3}Co_{0.2}]O_2$ with high initial specific capacity and good cycle performance by CHC method is found to be 820 °C. By comparison, for CCC method, such an optimal temperature is 860 °C, which is higher than the former. These results illustrate that the Li$[Ni_{0.5}Mn_{0.3}Co_{0.2}]O_2$ with optimal performance could be prepared at relatively low temperature by CHC method than by CCC method.

As well as operation at room temperature, the performance of the material at elevated temperatures is important. Therefore, it is significantly critical to concern the high-temperature characteristics of the prepared Li$[Ni_{0.5}Mn_{0.3}Co_{0.2}]O_2$. The initial charge/discharge profiles of the sample CHC-820 (which is among the best of the samples prepared by CHC method) and CCC-860 (which is among the best of the samples prepared by CCC method) at 0.2 C rate between 3.0 and 4.3 V vs. Li^+/Li at 55 °C are shown in Fig. 10, and the corresponding cycle performances are displayed in Fig. 11. It can be seen from

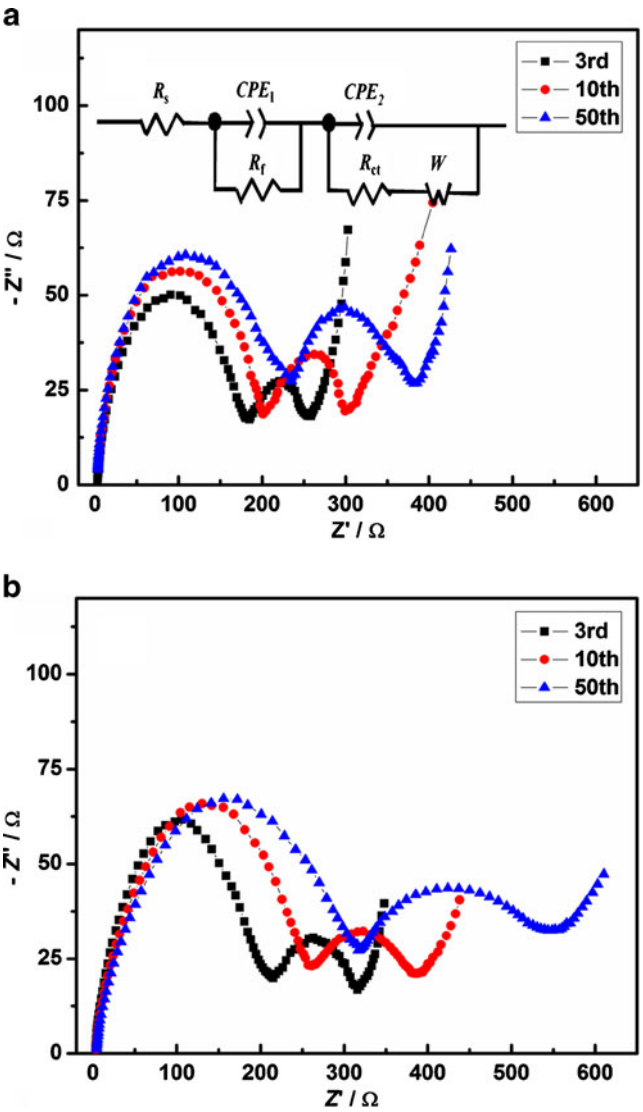

Fig. 12 Nyquist plots of sample **a** CHC-820 and **b** CCC-860 at different cycle stages. The *insert*: the schematic representation of equivalent circuit

Table 2 Simulated parameters using equivalent circuit in Fig. 12a

Resistance parameters	CHC-820			CCC-860		
	Third	Tenth	50th	Third	Tenth	50th
R_s (Ω)	2.9	3.2	3.5	3.0	3.5	4.4
R_{sf} (Ω)	180.5	197.8	231.5	212.2	252.2	315.2
R_{ct} (Ω)	75.2	100.2	151.3	97.5	129.4	231.7

Fig. 10 that the reversible capacities for both samples increase when the cells were cycled at 55 °C. The initial discharge capacities of 180 and 173.6 mAh g^{-1} can be obtained for the sample CHC-820 and CCC-860, respectively. This phenomenon is consistent with the previous results reported by Ohzuku et al. [22], and they considered that the increase in rechargeable capacity should be attributed to the negative shift of reversible potential as a function of temperature, not kinetic effect. As being shown in Fig. 11, both the samples exhibit slightly low capacity retention as compared with room temperature. The capacity retentions of sample CHC-820 and CCC-860 are 96.7 % and 93.9 %, respectively.

To explain the reason for the different cyclical stability of samples CHC-820 and CCC-860, the electrochemical impedance spectroscopy was carried out for the two samples at different cycle numbers after being charged to 4.3 V. The corresponding Nyquist plots are given in Fig. 12. The intercept at the Z_{real} axis in high frequency refers to R_s, which includes electrolyte solution resistance, electric contacts resistance, and ion conductive resistance. The semi-circle in the high frequency range is due to the surface film resistance (R_f); the semicircle in the middle frequency range reflects the charge transfer resistance (R_{ct}); and the sloping line in the lower frequency represents lithium-ion diffusion resistance in electrode bulk, namely the Warburg impedance. The non-linear least squares fitting procedure from B.A. Boukamp [23] was used to simulate the impedance data; the equivalent circuit was given in Fig. 15a, and the results are listed in Table 2. It can be seen that the R_f and R_{ct} of CCC-860 increase with increasing in cycle numbers. However, in contrast

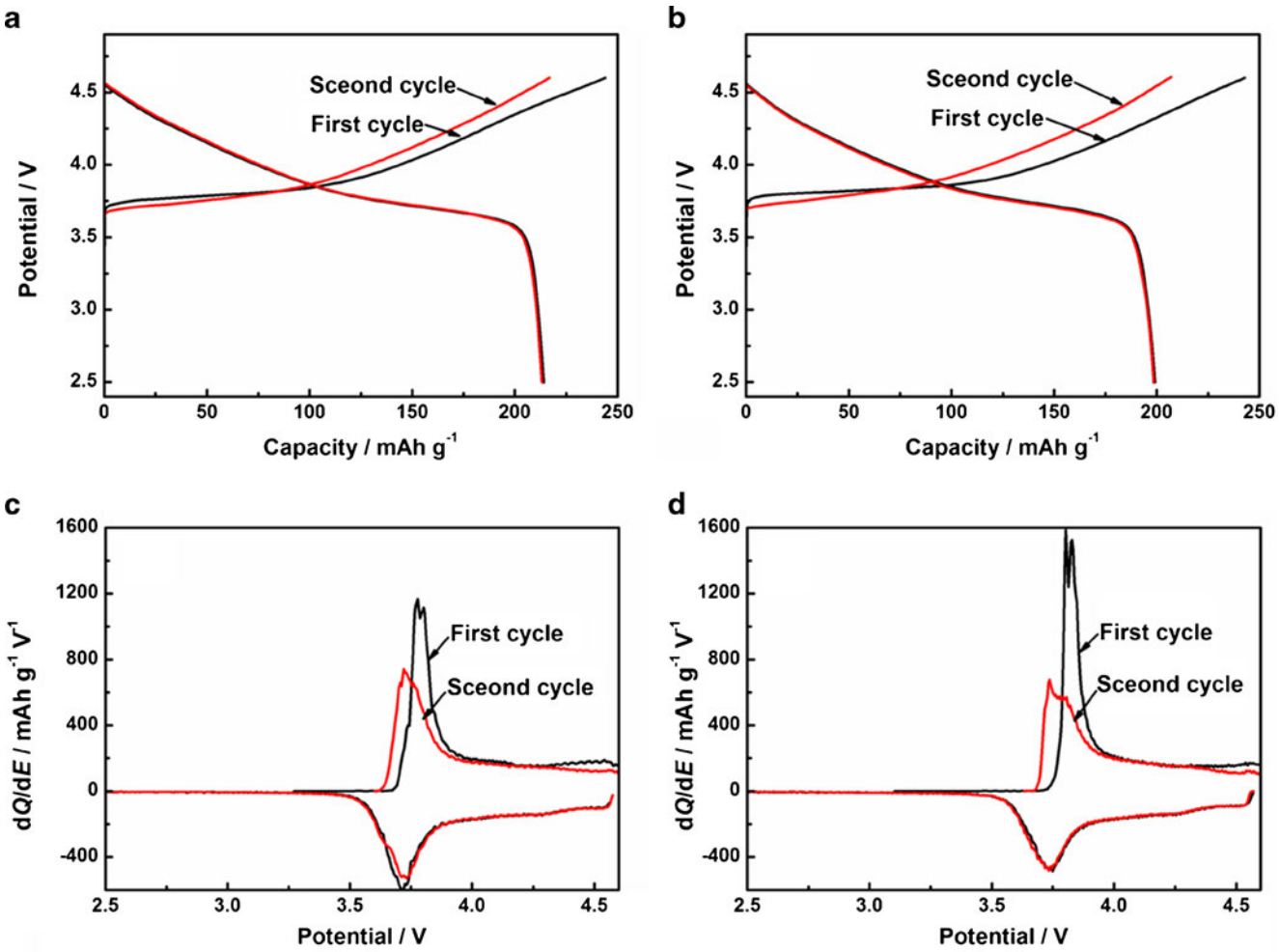

Fig. 13 The first and second charge/discharge profiles for sample **a** CHC-820 and **b** CCC-860. Differential capacity ($\partial Q/\partial E$) vs. cell potential of the Li/Li[$Ni_{0.5}Mn_{0.3}Co_{0.2}$]O_2 coin cell corresponding to the first and second charge and discharge curves of sample **c** CHC-820 and **d** CCC-860

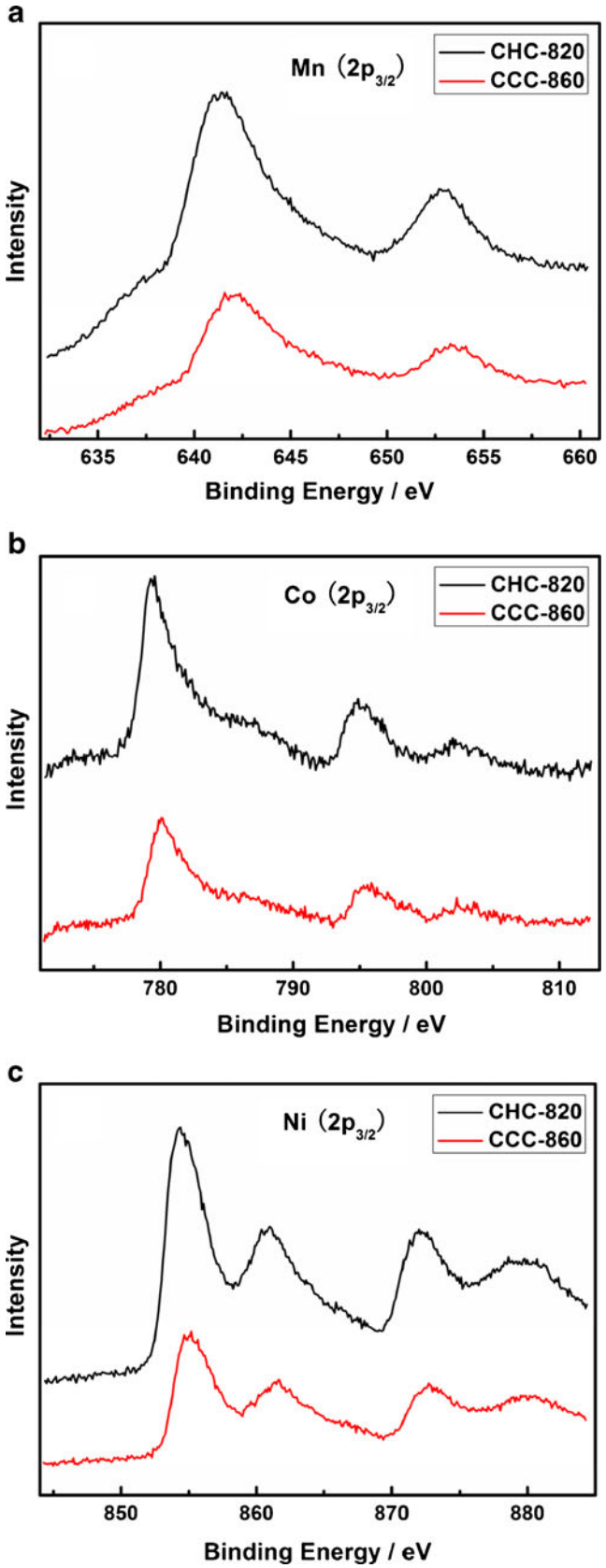

Fig. 14 XPS emission spectra of **a** Mn $2p_{3/2}$, **b** Co $2p_{3/2}$, and **c** Ni $2p_{3/2}$ in the $Li[Ni_{0.5}Mn_{0.3}Co_{0.2}]O_2$

with CCC-860, the CHC-820 shows the smaller total resistance (sum of surface layer resistance and charge transfer resistance) and relative stable R_f and R_{ct} values upon charge and discharge cycles, which guarantees the better cycle stability.

$Li[Ni_{1-x-y}Mn_xCo_y]O_2$ is only partially de-intercalated and intercalated when cells are charged and discharged in the voltage range of 3.0–4.3 V vs. Li^+/Li. Higher discharge capacities can be obtained when the voltage range is broadened. Here, in order to investigate the characteristic of the lithium ion de-intercalated and intercalated to the $Li[Ni_{0.5}Mn_{0.3}Co_{0.2}]O_2$ host in a wide voltage range, 4.6 V vs. Li^+/Li is chosen as the upper limit because the critical upper limit of $LiNiO_2$ and $LiCoO_2$ is 4.6 V [24]. The cells using CHC-820 and CCC-860 as the active material were operated at the 0.2 C rate in the voltage range of 2.5–4.6 V vs. Li^+/Li at 25 °C. The first and second charge/discharge cycle profiles and differential capacity profiles of the sample CHC-820 and CCC-860 are presented in Fig. 13. It can be seen from Fig. 13a and b that the initial discharge capacities are remarkably increased while the voltage range is broadened; the discharge capacities of 214.3 and 199.1 mAh g^{-1} can be obtained for the sample CHC-820 and CCC-860 at the first cycle. It is well known that the series $Li[Ni_{0.5}Mn_{0.5})_{1-x}Co_x]O_2$ materials (including $Li[Ni_{1/3}Co_{1/3}Mn_{1/3}]O_2$, $Li[Ni_{0.4}Mn_{0.4}Co_{0.2}]O_2$, and $Li[Ni_{0.5}Mn_{0.5}]O_2$) usually show two couples of redox peaks during the charge and discharge cycle. The first couple of redox peaks is sharp and centered at about 3.75 V vs. Li^+/Li; the other is small and centered at about 4.5 V vs. Li^+/Li. They are ascribed to Ni^{2+}/Ni^{4+} and Co^{3+}/Co^{4+} redox couples [6, 10], respectively. However, it can be seen from Fig. 13c, d that the samples CHC-820 and CCC-860 show three anodic peaks and two cathodic peaks during the first cycle. Three anodic peaks at about 3.75, 3.80, and 4.55 V vs. Li^+/Li is probably identified as Ni^{2+}/Ni^{3+}, Ni^{3+}/Ni^{4+} and Co^{3+}/Co^{4+} redox couple, respectively, while two cathodic peaks at about 3.74 and 4.53 V vs. Li^+/Li match along with Ni^{4+}/Ni^{2+} and Co^{4+}/Co^{3+} redox, respectively [25, 26]. In the second cycle, the first anodic peak at about 3.75 V vs. Li^+/Li increases while the second anodic peak at about 3.8 V vs. Li^+/Li degrades; two shoulder peaks have emerged into one broadened peak. In order to analyze the chemical composition of $Li[Ni_{0.5}Mn_{0.3}Co_{0.2}]O_2$ compound, the samples CHC-820 and CCC-860 were characterized by X-ray photoemission spectroscopy (XPS), and corresponding magnified Mn $2p_{3/2}$, Co $2p_{3/2}$, and Ni $2p_{3/2}$ are presented in Fig. 14. As illustrated in Fig. 14a, the binding energy of Mn $2p_{3/2}$ electron in $Li[Ni_{0.5}Mn_{0.3}Co_{0.2}]O_2$ is located at about 614.5 eV, which is the same as that of the Li_2MnO_3. These results suggest that the valence of Mn in both samples is tetravalent, well consistent with those reported [27]. It can be seen from Fig. 14b that the Co $2p_{3/2}$ has a characteristic peak with a binding energy of about 779.5 eV and can be indexed to the Co^{3+} (the published binding energy of a trivalent Co $2p_{3/2}$ electron is 779.3–779.9 eV [28]). As shown in

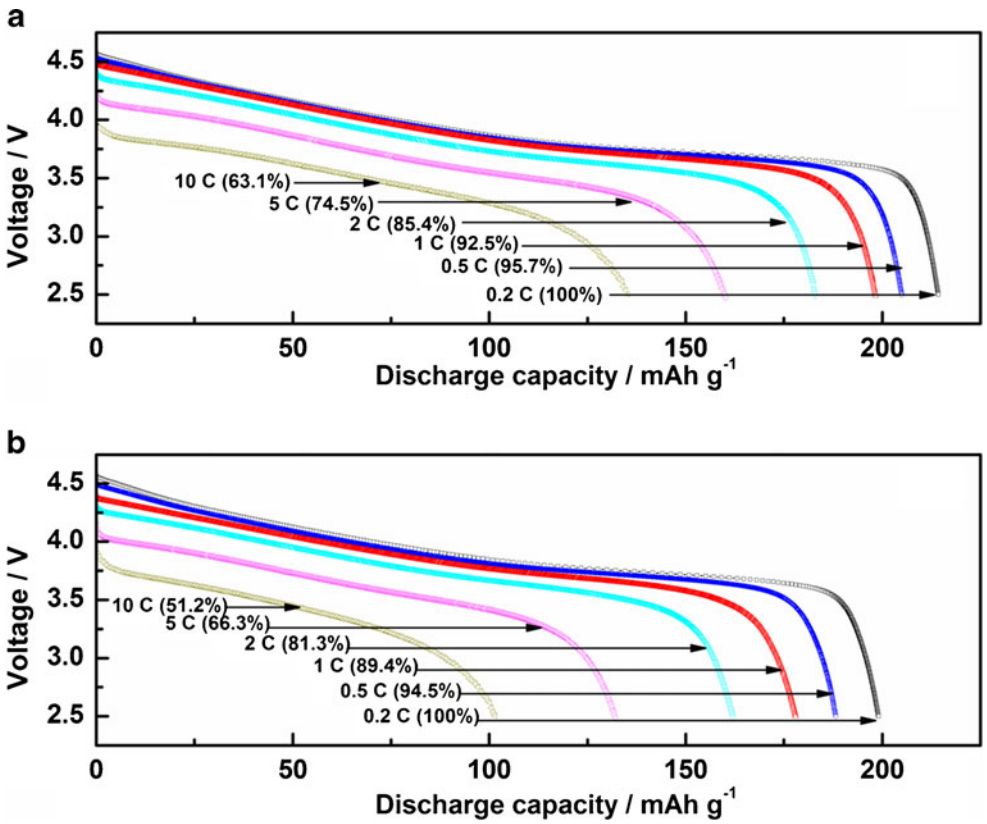

Fig. 15 Typical discharge curves of sample **a** CHC-820 and **b** CCC-860 at 0.2 C, 0.5 C, 1 C, 2 C, 5 C, and 10 C rates between 2.5 and 4.6 V at 25 °C

Fig. 14c, the Ni $2p_{3/2}$ peak is observed at approximately 855.5 eV. Because the standard binding energies of Ni^{2+} and Ni^{3+} are 853.8 and 857.3 eV [29], respectively, it is expected that the valence number of Ni in $Li[Ni_{0.5}Mn_{0.3}Co_{0.2}]O_2$ is a mixture of 2+ and 3+. Because the Mn^{4+} is inactive over the voltage range of 2.5–4.6 V vs. Li^+/Li, the first charge reaction should correspond to Ni^{2+}/Ni^{3+}, Ni^{3+}/Ni^{4+} and Co^{3+}/Co^{4+} redox couples. These results were well consistent with the previous reports by Delmas et al. and Liao et al. [30, 31]. Furthermore, it can be also noticed that the sample CHC-820 displays the sharper redox peak and smaller peak potential differences (ΔE) between oxidation and reduction peaks positions than the sample CCC-860 during the second cycle, suggesting that the better reversibility of Li de-intercalation processes occur in the cell of sample CHC-820 which, in turn, ensures a reduced capacity fade during battery cycling process.

To evaluate the rate capability of sample CHC-820 and CCC-860, the cells were first charged galvanostatically with a 0.2 C rate before each discharge testing and then discharged at different C rates from 0.2 to 10 C rates stepwise, every step lasted five charge/discharge cycles. Typical discharge curves of $Li/Li[Ni_{0.5}Mn_{0.3}Co_{0.2}]O_2$ cells at 0.2 C, 0.5 C, 1 C, 2 C, 5 C, and 10 C rates between 2.5 and 4.6 V vs. Li^+/Li are shown in Fig. 15. As shown in Fig. 15, the discharge capacity and average discharging voltage of the CCC-860 prepared from CCC method decreased with increasing current density. The capacity reached 94.5 %, 89.4 %, 81.3 %, 66.3 %, and 51.2 % at 0.5 C, 1 C, 2 C, 5 C, and 10 C compared with the specific capacity of 199.1 mAh g^{-1} at 0.2 C rate, respectively. By contrast, the decrease of capacity of the sample CHC-820 prepared from CHC method is less than that of the former when the discharging current is increased from 0.2 C to 10 C. It could be found that the sample CHC-820 delivers a discharge capacity of 205 mAh g^{-1} at 0.5 C (the capacity retention rate is about 95.7 % of that of 0.2 C), 198.3 mAh g^{-1} at 1 C (the capacity retention rate is about 92.5 % of that of 0.2 C), 183.1 mAh g^{-1} at 2 C (the capacity retention rate is about 85.4 % of that of 0.2 C), and 160.1 mAh g^{-1} at 5 C (the capacity retention rate is about 74.5 % of that of 0.2 C). Even at 10 C, the capacity of sample CHC-820 is still as high as 135.2 mAh g^{-1}, and the capacity retention rate is about 63.1 % of that of 0.2 C.

Table 3 Comparing the structure parameters and tap density of Li $[Ni_{0.5}Mn_{0.3}Co_{0.2}]O_2$ prepared by different methods

Sample	*a*-axis (Å)	*c*-axis (Å)	Unit volume (Å^3)	*c*/*a*	I_{003}/I_{104}
CHC-820	2.870	14.256	101.690	4.967	1.779
[8]	~2.87	~14.26	~102	~4.963	1.20
[9]	2.8721	14.2576	101.851	4.964	–
[11]	2.908	14.250	104.4	4.90	1.50

Table 4 Comparing the cycling performance of $Li[Ni_{0.5}Mn_{0.3}Co_{0.2}]O_2$ prepared by different methods

Sample	Capacity (mAh/g)		Capacity fade (%)	Current rate/density	Potential range (V)
	First cycle	*n*th cycle			
CHC-820	175.2	173.1(50)	1.2	32 mA/g	3.0–4.3
$LiNi_{1-x-y}Co_xMn_yO_2$ (x=0.2, y=0.3) [11]	140	113(14)	19.3	0.2 mA/cm^2	2.75–4.2
$LiNi_{0.5}Mn_{0.5-x}Co_xO_2$ (x=0.2) [8]	172	151(25)	14	40 mA/g	3.0–4.6

Compared with the layered $Li[Ni_{0.5}Mn_{0.3}Co_{0.2}]O_2$ prepared traditionally by mixed hydroxide method and solid-state reaction in the previous reports [7–9, 11], the sample CHC-820 prepared by continuous hydroxide co-precipitation not only shows a better structural integrity (as shown in Table 3) but also evident improvement on electrochemical performance (as shown in Table 4).

Conclusions

Spherical $Li[Ni_{0.5}Mn_{0.3}Co_{0.2}]O_2$ without any impurity phase was prepared by both the continuous hydroxide co-precipitation and continuous carbonate co-precipitation. The difference in preparation method results in the differences of the morphology (shape, particle size, and tap density) and structure stability of the compound, thereby influencing their electrochemical characteristics. The calcined temperature has little influence on the calculated structure parameters, spherical morphology, and reversible capacity of the sample prepared by hydroxide co-precipitation method while pronounced in the case of those prepared by the continuous carbonate co-precipitation method. Comparatively, continuous hydroxide co-precipitation is much more suitable for preparing spherical $Li[Ni_{0.5}Mn_{0.3}Co_{0.2}]O_2$ cathode material with high tap density, hexagonal layered structure, and excellent electrochemical performance. The optimal $Li[Ni_{0.5}Mn_{0.3}Co_{0.2}]O_2$ prepared by this method at 820 °C shows not only a better structural integrity (higher ratio of I_{003} /I_{104}) but also evident improvement on electrochemical performance. It delivers high initial discharge capacity of 175.2 mAh g^{-1} at 0.2 C rate between 3.0 and 4.3 V vs. Li^+/Li, and the capacity retention of 98.8 % can be retained after 50 cycles. While the voltage range is broadened up to 2.5 and 4.6 V vs. Li^+/Li, the special discharge capacity at 0.2 C reaches 214.3 mAh g^{-1}, and the capacity retention percentages at 0.5 C, 1 C, 2 C, 5 C, and 10 C based on 0.2 C are 95.7 %, 92.5 %, 85.4 %, 74.5 %, and 63.1 %, respectively.

Therefore, it is concluded that the spherical $Li[Ni_{0.5}Mn_{0.3}Co_{0.2}]O_2$ prepared by the continuous hydroxide co-precipitation method can be used as a possible alternative cathode material in response to an expanding need for the advanced lithium-ion batteries.

Acknowledgments This work was funded by the National Natural Science Foundation of China under project No. 20871101, Scientific and Technological Plan project of Ministry of Science and Technology no. 2009GJD20021, Scientific Research Fund of Hunan Provincial Education Department no. 09C947, Key Project of Science and Technology Department of Hunan Province Government under project no. 2009WK2007, colleges, and universities in Hunan Province plans to graduate research and innovation under project no. CX2009B133.

References

1. Meng XL, Dou SM, Wang WL (2008) J Power Sources 184:489–493
2. Lee K-S, Myung S-T, Moon J-S, Sun Y-K (2008) Electrochim Acta 53:6033–6037
3. Xiao L, Liu XJ, Zhao X, Liang HX, Liu HX (2011) Solid State Ionics 192:335–338
4. Martha SK, Sclar H, Framowitz ZS, Kovacheva D, Saliyski N, Gofer Y, Sharon P, Golik E, Markovsky B, Aurbach D (2009) J Power Sources 189:248–255
5. Periasamy P, Kalaiselvi N (2006) J Power Sources 159:1360–1364
6. Lin HC, Zheng JM, Yang Y (2010) Mater Chem Phys 119:519–523
7. Li DC, Sasaki Y, Kobayakawa K, Sato Y (2006) Electrochim Acta 51:3809–3813
8. Li DC, Sasaki Y, Kageyama M, Kobayakawa K, Sato Y (2005) J Power Sources 148:85–89
9. Kim S-B, Lee KJ, Choi WJ, Kim W-S, Jang IC, Lim HH, Lee YS (2010) J Solid State Electrochem 14:919–922
10. Myung S-T, Ogata A, Lee K-S, Komaba S, Sun Y-K, Yashiro H (2008) J Electrochem Soc 155:A374–A383
11. Liu ZL, Yu AS, Lee JY (1999) J Power Sources 81–82:416–419
12. Yang SY, Wang XY, Yang XK, Liu L, Liu ZL, Bai YS, Wang YP (2011) J Solid State Electrochem. doi:10.1007/s10008-011-1513-6
13. Yang SY, Wang XY, Chen QQ, Yang XK, Li JJ, Wei QL (2011) J Solid State Electrochem. doi:10.1007/s10008-011-1356-1
14. Joint Committee on Powder Diffraction Standards, card no. 03–0177
15. Park SH, Kang SH, Belharouak I, Sun YK, Amine K (2008) J Power Sources 177:177–183
16. Muñoz-Rojas D, Casas-Cabanas M, Baudrin E (2010) Solid State Ionics 181:536–544
17. Gibot P, Casas-Cabanas M, Laffont L, Levasseur S, Carlach P, Hamelet S, Tarascon JM, Masquelier C (2008) Nat Mater 7:741–747
18. Reimers JN, Rossen E, Jones CD, Dahn JR (1993) Solid State Ionics 61:335–344
19. Luo XF, Wang XY, Liao L, Gamboa S, Sebastian PJ (2006) J Power Sources 158:654–658
20. Zhang S, Deng C, Yang SY, Niu H (2009) J Alloys Compd 484:519–523

21. Liang YG, Han XY, Zhou XW, Sun JT, Zhou YH (2007) Electrochem Commun 9:965–970
22. Yabuuchi N, Ohzuku T (2005) J Power Sources 146:636–639
23. Boukamp BA (1989) Equivalent circuit, user's manual. University of Twente, The Netherlands
24. Paulsen JM, Thomas CL, Dahn JR (2000) J Electrochem Soc 147:861–869
25. Li JG, Wang L, Zhang Q, He XM (2009) J Power Sources 189:28–33
26. Ni JF, Zhou HH, Chen JT, Zhang XX (2008) Electrochim Acta 53:3075–3083
27. Shaju KM, Subba Rao GV, Chowdari BVR (2002) Electrochim Acta 48:145–151
28. Madhavi S, Subba Rao GV, Chowdari BVR, Li SFY (2001) J Electrochem Soc 148:A1279–A1286
29. Sun YS, Ouyang CY, Wang ZX, Huang XJ, Chen LQ (2004) J Electrochem Soc 151:A504–A508
30. Delmas C, Menetrier M, Croguennec L, Saadoune I, Rougier A, Pouillerie C, Prado G, Grune M, Fournes L (1999) Electrochim Acta 45:243–253
31. Liao PY, Duh JG, Sheen SR (2005) J Electrochem Soc 152: A1695–A1700